PHILOSOPHICAL MAGAZINE, 2018
VOL. 98, NO. 14, 1256–1271
https://doi.org/10.1080/14786435.2018.1433884

Taylor & Francis
Taylor & Francis Group

Modelling of creep hysteresis in ferroelectrics

Xuan He[a], Dan Wang[a], Linxiang Wang[a] and Roderick Melnik[b]

[a]State Key Laboratory of Fluid Power and Mechatronic Systems, Zhejiang University, Hangzhou, China; [b]MS2Discovery Interdisciplinary Research Institute, Wilfrid Laurier University, Waterloo, Canada

ABSTRACT

In the current paper, a macroscopic model is proposed to simulate the hysteretic dynamics of ferroelectric ceramics with creep phenomenon incorporated. The creep phenomenon in the hysteretic dynamics is attributed to the rate-dependent characteristic of the polarisation switching processes induced in the materials. A non-convex Helmholtz free energy based on Landau theory is proposed to model the switching dynamics. The governing equation of single-crystal model is formulated by applying the Euler–Lagrange equation. The polycrystalline model is obtained by combining the single crystal dynamics with a density function which is constructed to model the weighted contributions of different grains with different principle axis orientations. In addition, numerical simulations of hysteretic dynamics with creep phenomenon are presented. Comparison of the numerical results and their experimental counterparts is also presented. It is shown that the creep phenomenon is captured precisely, validating the capability of the proposed model in a range of its potential applications.

ARTICLE HISTORY
Received 20 August 2017
Accepted 22 January 2018

KEYWORDS
Ferroelectrics; creep; polycrystalline; rate-dependent; hysteretic dynamics; Landau theory

1. Introduction

Ferroelectric materials have gained great interest from researchers around the world due to the intrinsic multi-field coupling effects since their discovery. They possess wide ranges of potential applications including high precision MEMS/NEMS sensors and actuators, efficient vibration dampers and energy harvesters, new generation random access memory devices, among others [1–6]. In traditional applications, the materials always operate in the linear piezoelectric range where a simple linear constitutive model can well capture the materials' behaviours [7,8]. However, to take full advantage of their potential, ferroelectrics need to be subject to substantially larger external electric fields and/or stresses, in which case, the nonlinear hysteretic phenomena have to be considered [9,10]. To compensate the hysteretic nonlinearities and optimise the material behaviours, an

CONTACT Linxiang Wang wanglx236@zju.edu.cn

efficient hysteresis model with high precision is especially important. Besides, to well understand and analyse the poling process, which is necessary for ferroelectric ceramics to obtain macroscopic piezoelectricity, an efficient and precise electromechanically coupled hysteresis model is also required [11,12].

In addition to the coupled hysteresis mentioned above, creep is another important phenomenon present in the material, which needs to be carefully analysed and modelled. In certain applications, such as high precision actuators, instead of a cyclic varying electric signal, input with a constant step is fed into the material. The outputs (both electrical and mechanical) will not stop varying instantaneously as the input signal. Instead, it will keep changing until reaching its saturation. This behaviour is in the heart of the creep phenomenon. Unlike mechanical creep with inelastic deformation, creep in ferroelectrics can be ascribed to the microscopic polarisation switching process induced in the material [13,14]. A well-constructed model should incorporate the ability to capture this phenomenon automatically or with very few modifications. However, in the literature, only a limited number of experimental investigations and theoretical modelling of this behaviour exist. The relationship between the creep phenomenon and underlying polarisation switching dynamics remains to be better understood [15].

Currently, the vast majority of the modelling strategies for ferroelectric materials can be grouped into two main categories. One is based on micromechanical models, and the other is on phenomenological ones. While micromechanical models can provide high precision for complicated load cases, phenomenological models are expected to be more efficient with respect to computational cost [16–18]. It is noticed that recently, the macroscopic phenomenological models have been used by several researchers to investigate the complicated nonlinear hysteretic electromechanically coupled process during poling, which can lead to a meaningful optimisation of the performance of ferroelectric ceramics [19,20]. However, as for applying the above models to study the creep phenomenon, a very few publications exist.

A hysteresis model for ferroelectric ceramics based on the analysis and modelling of the polarisation orientation switching process has been proposed by our research team in a recent publication [21]. The model can capture the coupled hysteresis involved in the material with a high precision and with a low-numerical cost. At the grain level, a coupled differential system has been formulated to simulate the polarisation switching process, which is intrinsically rate-dependent and electromechanically coupled. At the macroscopic level, the behaviours of the ceramics have been modelled as a weighed combination of the response of each grain with the help of a density function. The ability of the model to capture the rate-dependent minor loops has already been demonstrated in the publication. Here, we will further employ this model to simulate the creep hysteresis loop involved in ferroelectrics and discuss the underlying relationship between the macroscopic creep phenomenon and microscopic polarisation switching process, which will improve our understanding about the underline physical mechanism

behind the macroscopic behaviours of the material and improve the performance of the ferroelectric devices. The current paper is organised as follows. A brief introduction of the mechanism of polarisation switching and details of the current model are given in Section 2. Discussion of the rate-dependent characteristics of the current model, which are the basis for the analysis of creep phenomenon, is carried out in Section 3. Section 4 presents a detailed illustration of creep phenomenon with the current model. Finally, the numerical results of modelling creep phenomenon are discussed in Section 5. Concluding remarks are given in Section 6.

2. Hysteretic dynamics associated with polarisation switching

It is well accepted that hysteresis in ferroelectrics is mainly caused by the polarisation orientation switching. Besides, field-induced structural/phase changes also have an important contribution on the hysteretic properties of ferroelectrics, especially for ferroelectric ceramics near the morphotropic phase boundary [22,23]. For simplicity, only the polarisation switching in the tetragonal phase along a quasi one-dimensional direction is considered. In a quasi one-dimensional situation (Figure 1), the polarisation switching can be divided into two cases: 180° switching and non 180° switching. Non 180° switching can be induced by an external electric field or stress, while 180° switching can only be induced by an external electric field. The three different polarisation orientations in the material is treated as three phases (P_+, P_0 and P_-) by Landau theory [24]. A non-convex free energy function is constructed. Each local minimum of the energy function corresponds to a stable phase. The polarisation switching process is mimicked by the transition between different minima of the free energy function. Further details of the current model can be founded in Ref. [24]. It needs to be pointed out the current model is only a phenomenological model based on Landau theory, whose modelling capability will be demonstrated in the following part. Detailed discussion about the crystalline symmetry is not included. For related discussions about the crystalline symmetry on the basis of Landau theory, Refs. [23,25,26] can be referred to.

2.1. Single-crystal model

The governing equations of a single-crystal model can be derived by applying the Euler–Lagrange equation to the non-convex free energy function [24,27]. The obtained governing equations retain the following form [21]:

$$\begin{aligned} \tau_p \frac{\mathrm{d}P}{\mathrm{d}t} + a_2 P + a_4 P^3 + a_6 P^5 + 2b\varepsilon P - E = 0, \\ \tau_\varepsilon \frac{\mathrm{d}\varepsilon}{\mathrm{d}t} + k\varepsilon + bP^2 - \sigma = 0, \end{aligned} \tag{1}$$

where τ_p and τ_ε are the material-related parameters which capture the relaxation effects of the polarisation switching process. They are related to the rate-dependent

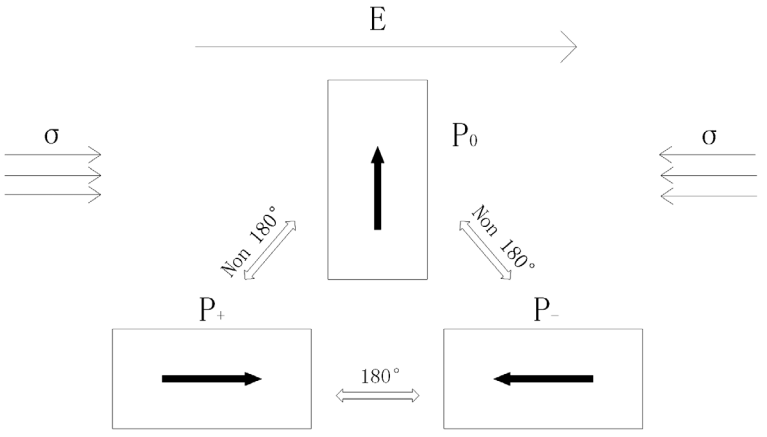

Figure 1. Sketch of polarisation orientation switching in a quasi-one-dimensional analogue.

characteristics of the material. a_2, a_4 and a_6 denote the Landau coefficients; b and k are the electromechanical coupling coefficient and linear elastic constant, respectively.

2.2. Polycrystalline model

In real applications, ferroelectrics usually exist in the form of ceramics rather than a single crystal. Thus, it is far from enough to employ the single-crystal model to capture the behaviours of ferroelectric ceramics. As mentioned in [21], the contribution of each single grain to the macroscopic ceramic properties is related to the angle θ between its principal axis and the direction of the applied electric field. Since the physical properties of each grain are assumed to be similar, the governing equations of a single grain can be written in the following form:

$$\begin{aligned} \tau_p \frac{\mathrm{d}P_\theta}{\mathrm{d}t} + a_2 P_\theta + a_4 P_\theta^3 + a_6 P_\theta^5 + 2b\varepsilon_\theta P_\theta - E\cos\theta = 0, \\ \tau_\varepsilon \frac{\mathrm{d}\varepsilon_\theta}{\mathrm{d}t} + k\varepsilon_\theta + bP_\theta^2 - \sigma\cos\theta = 0, \end{aligned} \tag{2}$$

where P_θ and ε_θ represent the local polarisation and strain in the single grian, respectively.

The macroscopic dynamics of the materials can be treated as a combination of the dynamics of all single grains. Polarisation and strain of the ceramics are further expressed as follows:

$$\begin{aligned} P = \int_\theta P_\theta w(\theta)\cos\theta \cdot \mathrm{d}\theta = \int_\theta P_\theta \lambda(\theta) \cdot \mathrm{d}\theta, \\ \varepsilon = \int_\theta \varepsilon_\theta w(\theta)\cos\theta \cdot \mathrm{d}\theta = \int_\theta \varepsilon_\theta \lambda(\theta) \cdot \mathrm{d}\theta, \end{aligned} \tag{3}$$

where $w(\theta)$ is the volume percentage of grains with the angle θ between the principal axis and the applied field. In order to simplify our model and numerical

calculation, a density function $\lambda(\theta)$, taking into account the influence of both $w(\theta)$ and $cos\theta$, is introduced. In addition, the above equations can be reformulated in a discrete form by using Gaussian quadrature technique:

$$\begin{aligned} P &= \int_\theta P_\theta \lambda(\theta) \cdot \mathrm{d}\theta = \sum_{i=1}^{M} P_i \lambda\left(\theta_i\right) w_i = \sum_{i=1}^{M} P_i W_i, \\ \varepsilon &= \int_\theta \varepsilon_\theta \lambda(\theta) \cdot \mathrm{d}\theta = \sum_{i=1}^{M} \varepsilon_i \lambda\left(\theta_i\right) w_i = \sum_{i=1}^{M} \varepsilon_i W_i, \end{aligned} \tag{4}$$

where M is the number of representative single grains. In Equation (4), w_i is the ith weight coefficient for the Gaussian quadrature approximation; W_i is a new coefficient that includes the effect of both w_i and $\lambda\left(\theta_i\right)$. To further simplify the model, W_i is treated as a new density function. Finally, the governing functions can be formulated as the following:

$$\begin{aligned} \tau_p \tfrac{\mathrm{d}P_i}{\mathrm{d}t} + a_2 P_i + a_4 P_i^3 + a_6 P_i^5 + 2b\varepsilon_i P_i - E\cos\theta_i = 0, \\ \tau_\varepsilon \tfrac{\mathrm{d}\varepsilon_i}{\mathrm{d}t} + k\varepsilon_i + bP_i^2 - \sigma\cos\theta_i = 0, \\ P = \sum_{i=1}^{M} P_i W_i, \\ \varepsilon = \sum_{i=1}^{M} \varepsilon_i W_i. \end{aligned} \tag{5}$$

3. Rate-dependent characteristic

According to Landau theory, a hysteresis loop can be sketched from a polynomial constitutive curve, see Figure 2 [27]. As the external field varies, the polarisation switches from A to B or C to D since the states on the solid constitutive curve between points A and C are unstable. Furthermore, the phenomenon of polarisation switching is a rate-dependent process which means different switching behaviours will be present in the macroscopic hysteresis loop with different input rates as illustrated in Figure 2. As the rate increases, the switching curve will change from $\widehat{\mathrm{AB}}$ to $\widehat{\mathrm{AB''}}$ as well as from $\widehat{\mathrm{CD}}$ to $\widehat{\mathrm{AB''}}$. A fatter hysteresis loop is present.

The current model performs well in capturing the rate-dependent hysteretic dynamics. The simulated hysteresis loops for the same material under different input rates are demonstrated in Figure 3. In addition, Figures 4 and 5 show the hysteresis loops for different materials with different τ_p and values under the same input electric field. The capability of this model for the rate-dependent minor loops has been demonstrated and discussed in Ref. [21]. The values of model parameters in rate-dependent simulations can be found in Table 1.

4. Creep phenomenon

A normal macroscopic loop between electric polarisation and external field is formed when ferroelectrics are subject to a cyclic electric field. However, in certain applications, the external loading is kept constant for some extended periods

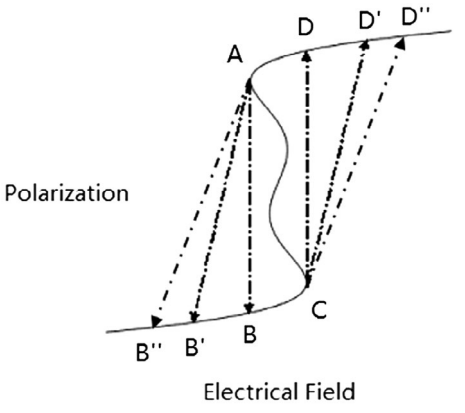

Figure 2. Illustrative diagram of single grain hysteresis loop.

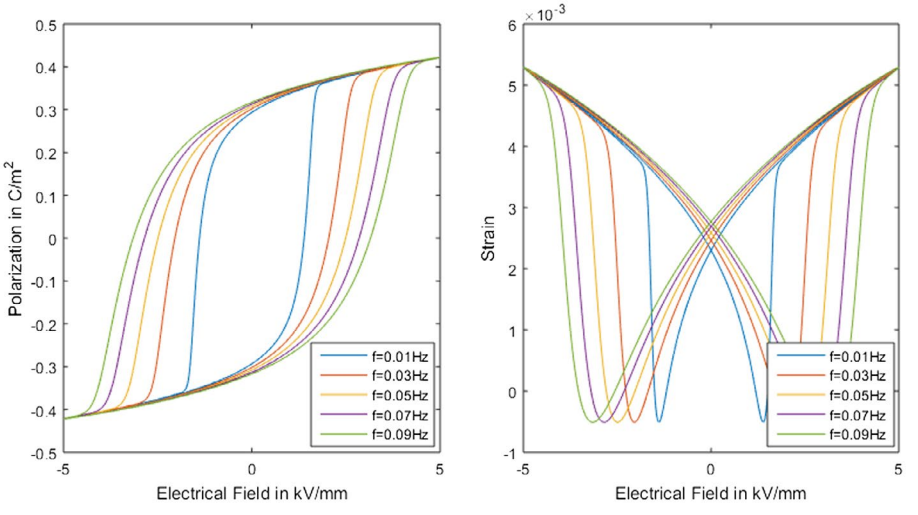

Figure 3. (colour online) Simulated hysteresis loops under different input frequencies.

of time, in which case, hysteresis loops with creep phenomenon will be present, as shown in Figure 6. In the following, an explanation based on the view of microscopic polarisation switching mechanism is provided. With the external field increasing from the negative minimum, the polarisation increases reversely first. As the electric field exceeds the minimum value of the effective coercive field involved in the material (E_0), the corresponding polarisation orientation switching takes place. Due to the time effect, it takes time for the polarisation to finish the switching process. As shown in Figure 7, the external field stops changing at E_1. If the time effect is not taken into consideration, the grains with effective coercive field less than E_1, that is the part corresponding to density a, would have finished the polarisation switching process. Thus, no more polarisation variation takes place, which means that no creep polarisation would be present. In fact, the polarisations corresponding to the density a will not finish the switching process.

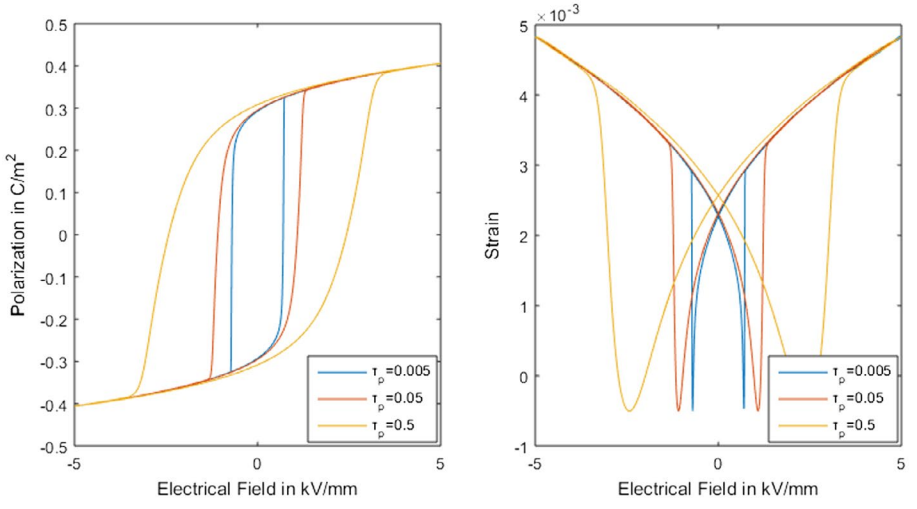

Figure 4. (colour online) Simulated hysteresis loops with different polarisation relaxation parameters τ_p.

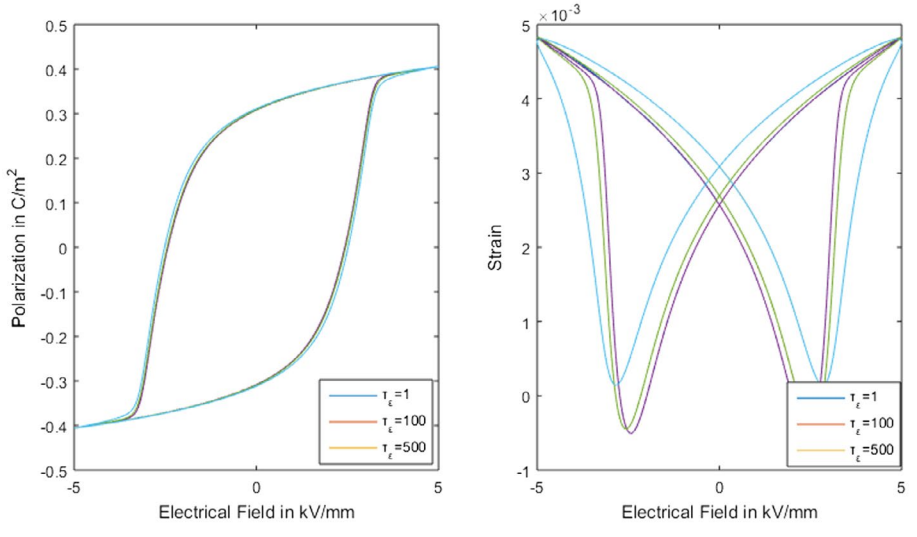

Figure 5. (colour online) Simulated hysteresis loops with different strain relaxation parameters τ_ε.

Only one portion of the polarisation variation in the figure (density *b*) has finished, while the other part of the polarisation (density *c*) has not finished. As the current model can well capture the rate-dependent effects, the creep phenomenon will be captured automatically (Figure 8).

5. Numerical simulation and validation

To demonstrate the capability of modelling creep hysteresis by the current model, two simulations have been carried out in the current paper. In particular, the

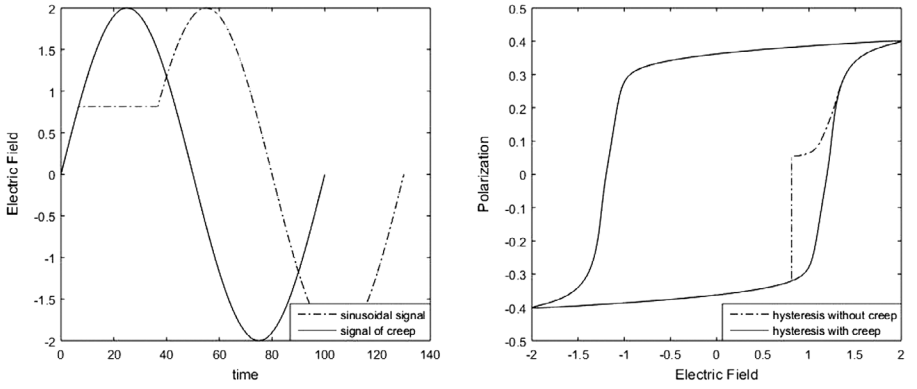

Figure 6. The signals and hysteresis loops for polycrystalline model with and without creep.

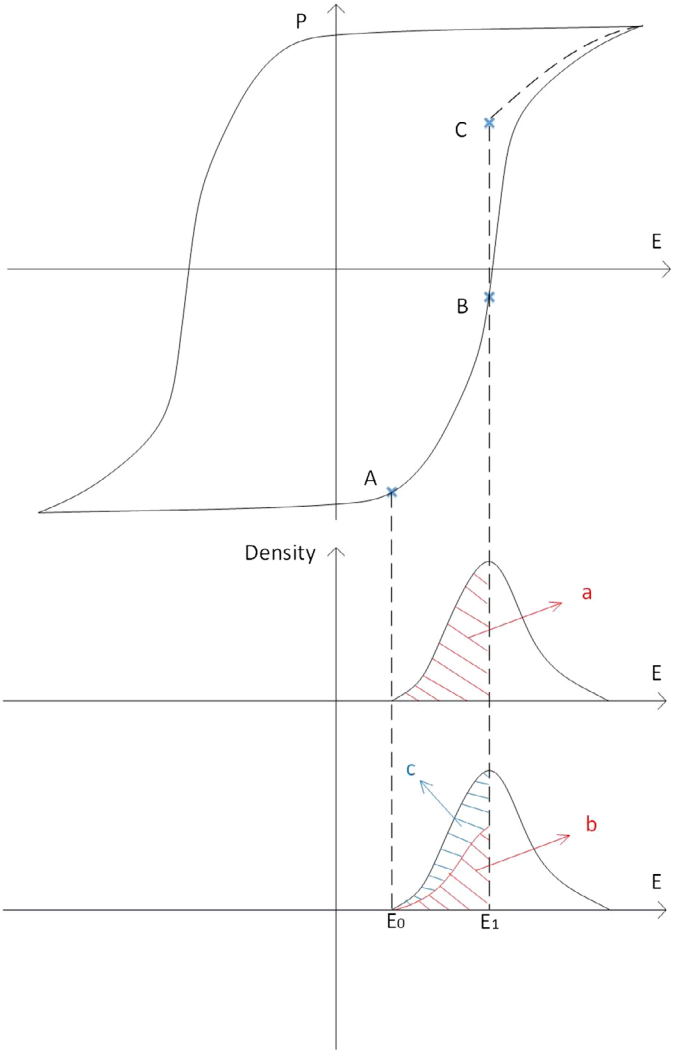

Figure 7. (colour online) Illustrations of the construction of creep.

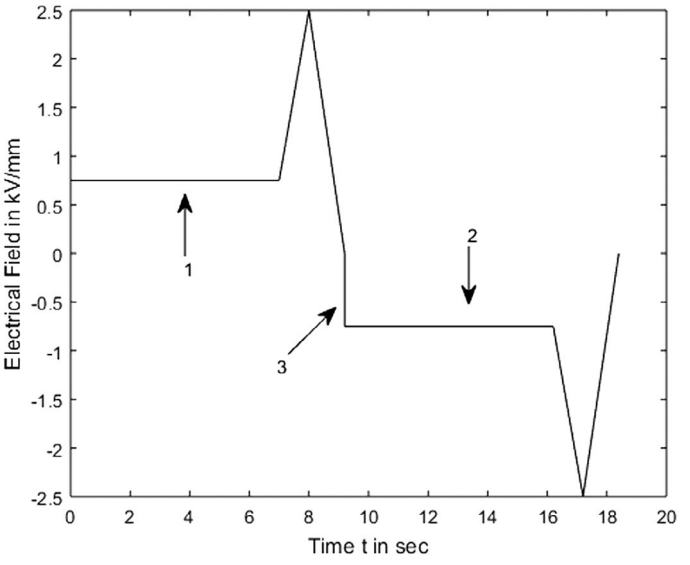

Figure 8. Excitation signal for the first creep experiment.

material Pz27 [28] is chosen for the decoupled system, and the material PIC 151 [29] is chosen for the coupled system. In the current model, the single crystal model parameters τ_p, τ_ε, a_2, a_4, a_6, b and k, as well as density values W_i at each θ_i point, need to be estimated (Table 1). As in Ref. [21], a simple log-normal density function is a good choice to approximate the density W_i:

$$W_i = \alpha e^{-[\ln(\theta_i/\gamma)/\beta]^2}, \tag{6}$$

where α, β and γ are newly-introduced material-related parameters that need to be fitted with experimental data. To obtain the unknown parameters, the following optimisation problem is carried out [21]:

$$\min_{mod.para.} G = \sum_{i=1}^{N} \left(\left(\frac{\widetilde{P}_i - P_i}{P_{magnitude}} \right)^2 + \left(\frac{\widetilde{\varepsilon}_i - \varepsilon_i}{\varepsilon_{magnitude}} \right)^2 \right), \tag{7}$$

where N is the number of data samples, $\widetilde{P}_i$ and $\widetilde{\varepsilon}_i$ are experimental results of the polarisation and strain, P_i and ε_i are the corresponding simulated values, and

Table 1. The values of the model parameters in rate-dependent simulations.

Parameter	Value
a_2	−4.9966
a_4	46.958
a_6	379.93
b	−334.59
k	10,266

$P_{magnitude}$ and $\varepsilon_{magnitude}$ are the magnitudes of the experimental data used to obtain the relative errors.

In a decouple system with only polarisation, the reduced governing equation and the optimisation problem can be written as follows:

$$\tau_p \frac{\mathrm{d}P_\theta}{\mathrm{d}t} + a_2 P_\theta + a_4 P_\theta^3 + a_6 P_\theta^5 - E\cos\theta = 0,$$

$$P = \sum_{i=1}^{M} P_i W_i, \tag{8}$$

$$\min_{mod.para.} G = \sum_{i=1}^{N} \left(\widetilde{P}_i - P_i\right)^2. \tag{9}$$

In the current paper, the built-in functions ode23t and fmincon in matlab 2015a have been employed to complete these numerical experiments.

5.1. Simulation results of the decoupled system

The experimental datasets in the first simulation are taken from Ref. [28]. In this simulation, the 500 θ values are evenly distributed in $[0, 0.4\pi]$. Furthermore, the following strategy is used to identify the parameters in the model: firstly, the single crystal model without denstiy funtion is identifed by using the experiment data to obtain the initial values for τ_p, a_2, a_4 and a_6; secondly, these obtained values are applied in the polycrystaline model to get the initial values of α, β and γ; finally, the full optimisation problems are carried out based on the strategy as described in Equation (9) to get the final parameters. The input electrical signal in the first experiment is shown in Figure 8. The initial values and optimised values are given in Table 2 and the density function is shown in Figure 9. Comparison between the simulted creep hysteresis loops and the experimental counterparts are illustrated in Figure 10. In addition, the variation of the creep polarisation during the holding time is further provided in Figure 11, where good modelling performance is demonstrated.

5.2. Simulation results of the coupled system

The experimental datasets in the second simulation are taken from Ref. [29]. In this simulation, the 500 θ values are evenly distributed in $[0, 0.38\pi]$. The parameter identification strategy in the coupled system is almost identical to the one in Section 5.1, but we need to first identify the initial values of b and k with the following reduced relation [21]:

$$\varepsilon = -\frac{b}{k}P^2 + \frac{\sigma}{k}. \tag{10}$$

Table 2. The initial values and optimised values of the model parameters in the first simulation.

Parameter	Initial value	Optimised value
τ_p	0.49999	0.47089
a_2	5.1001	4.8032
a_4	−219.89	−183.69
a_6	1542.9	1143.2
α	0.0034225	0.0049716
β	0.60005	0.85439
γ	0.44005	0.27797

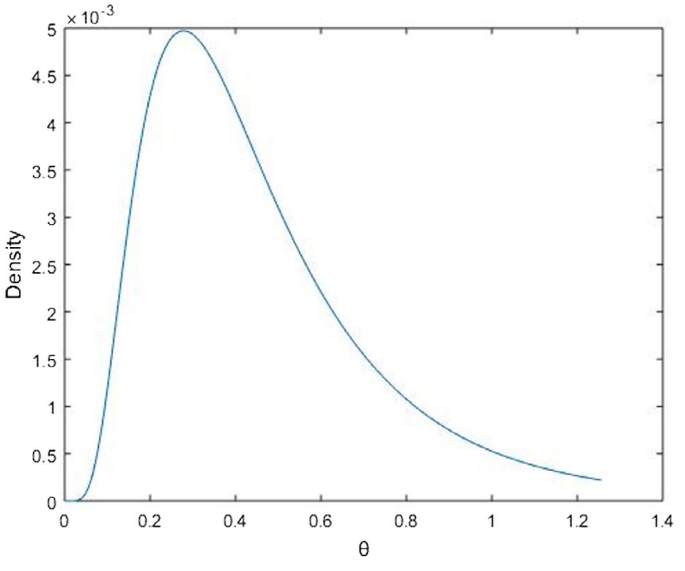

Figure 9. (colour online) The density function for the first simulation where α is 0.0049716, β is 0.85439 and γ is 0.27797.

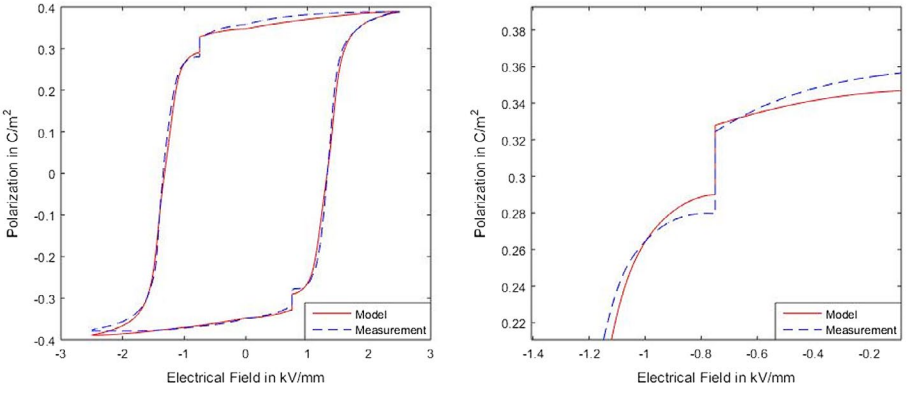

Figure 10. (colour online) (a) The polarisation hysteresis for the first simulation, measurements compared with simulations; (b) details of the creep phenomenon.

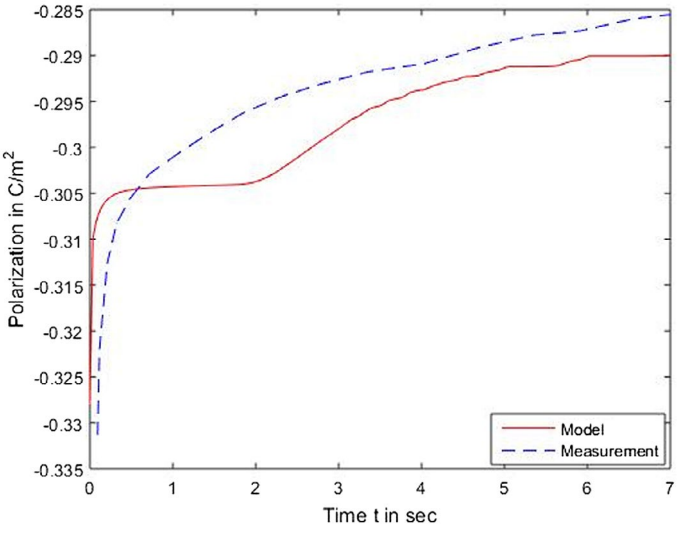

Figure 11. (colour online) Polarisation variations during the holding time for the first simulation.

The input electrical signal in the second experiment is shown in Figure 12. The initial values and optimised values are given in Table 3 and the density function is shown in Figure 13. The numerical result of hysteresis with a bias stress of 5.2 Mpa is shown in Figure 14 and its polarisation signals during holding in position 1, 2 and 3 are shown in Figure 15. It can be seen in Figure 14 that all 6 creep phenomena are well-captured by the current model, especially in the polarisation-field curve. However, the simulated strain-field curve is not as good

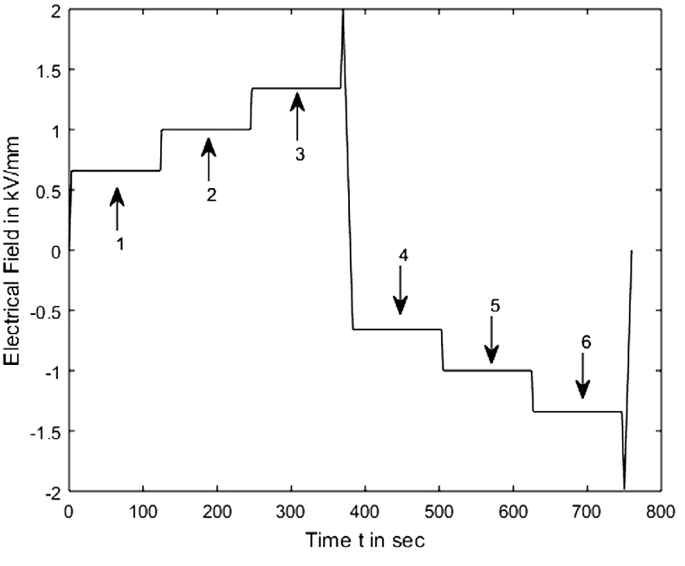

Figure 12. Excitation signal for the second creep experiment.

Table 3. The initial values and optimised values of the model parameters in the second simulation.

Parameter	Initial value	Optimised value
τ_p	5.0000	5.2430
a_2	−5.1050	−4.9966
a_4	50.082	46.958
a_6	422.98	379.93
τ_ε	5.0000	5.1012
b	−341.85	−334.59
k	10,000	10,266
α	0.0046094	0.0051681
β	0.56150	0.52448
γ	0.49240	0.46518

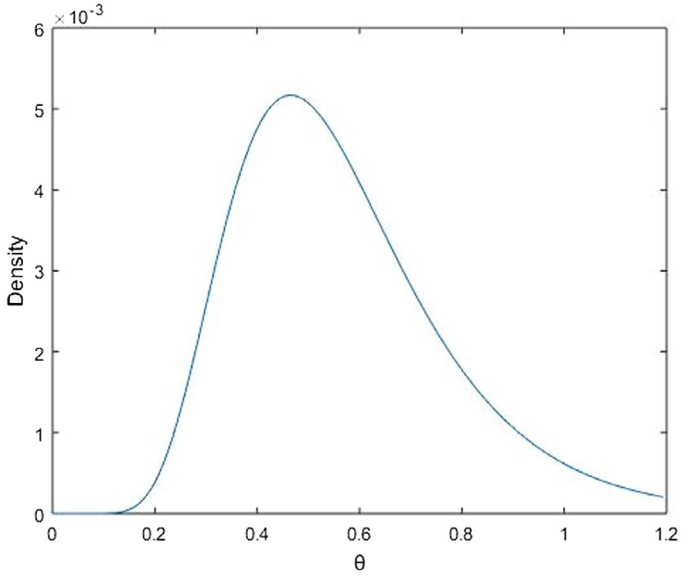

Figure 13. (colour online) The density function for the second simulation where α is 0.0051681, β is 0.52448 and γ is 0.46518.

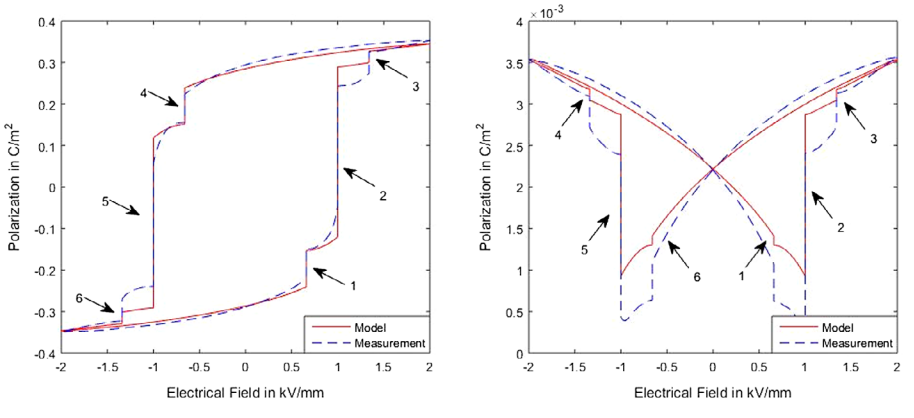

Figure 14. (colour online) The hysteresis curves for the second simulation, measurements compared with simulations: (a) polarisation and (b) strain.

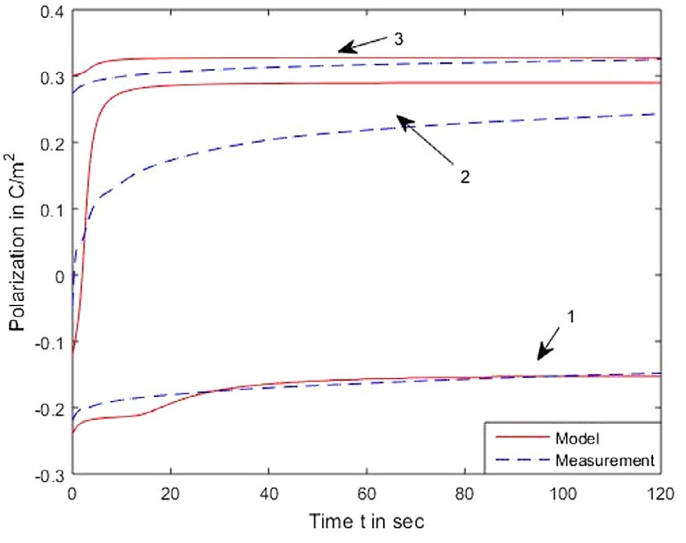

Figure 15. (colour online) Polarisation variations during the holding time for the second simulation.

as the polarisation-field curve, which means that there is still room for further improvement of this model.

6. Conclusion

In this paper, a macroscopic phenomenological model for ferroelectric hysteresis has been developed. The single-crystal governing equations have been obtained by applying the Euler–Lagrange equation, and the polycrystalline model has been obtained by combining the single-crystal dynamics with a density function. The developed model has been applied to demonstrate the creep phenomenon in the hysteretic dynamics, which is attributed to the rate-dependent characteristic of the polarisation switching process induced in the materials. Besides, the parameter identification strategies based on the current model have been presented. Creep phenomenon of hysteresis loop in polarisation is successfully simulated by the proposed, which is validated by the comparison between the experiment data and the simulated counterparts.

Disclosure statement

No potential conflict of interest was reported by the authors.

Funding

This work was supported by the National Natural Science Foundation of China [grant number 51575478], [grant number 61571007]; the National Sciences and Engineering Research Council (NSERC) of Canada; and the Canada Research Chair Program.

References

[1] C.R. Bowen, H.A. Kim, P.M. Weaver, and S. Dunn, *Piezoelectric and ferroelectric materials and structures for energy harvesting applications*, Energy Environ. Sci. 7(1) (2014), pp. 25–44.

[2] M. Ueda, Y. Kaneko, N. Yu, and A. Omote, *Battery-less shock-recording device consisting of a piezoelectric sensor and a ferroelectric-gate field-effect transistor*, Sensor Actuat. A-Phys. 232 (2015), pp. 75–83.

[3] V. Garcia and M. Bibes, *Ferroelectric tunnel junctions for information storage and processing*, Nat Commun. 5 (2014), p. 4289.

[4] Z.N. Ahmadabadi and S.E. Khadem, *Nonlinear vibration control and energy harvesting of a beam using a nonlinear energy sink and a piezoelectric device*, J. Sound Vib. 333(19) (2014), pp. 4444–4457.

[5] B. Lossouarn, M. Aucejo, and J.F. Deü, *Multimodal coupling of periodic lattices and application to rod vibration damping with a piezoelectric network*, Smart Mater. Struct. 24(4) (2015), pp. 1–13.

[6] R. Merry, R.V.D. Molengraft, and M. Steinbuch, *Modeling of a walking piezo actuator*, Sensor Actuat. A-Phys. 162(1) (2010), pp. 51–60.

[7] K.G. Webber, D.J. Franzbach, and J. Koruza, Determination of the true operational range of a piezoelectric actuator, J. Am. Ceram. Soc. 97(9) (2014), pp. 2842–2849.

[8] J.W. Judy, D.L. Polla, and W.P. Robbins, *A linear piezoelectric stepper motor with submicrometer step size and centimeter travel range*, IEEE Trans. Ultrason. Ferroelectr. Freq. Control 37(5) (1990), pp. 428–437.

[9] W. Lu, D.N. Fang, C.Q. Li, and K.C. Hwang, *Nonlinear electric–mechanical behavior and micromechanics modelling of ferroelectric domain evolution*, Acta Mater. 47(10) (1999), pp. 2913–2926.

[10] D.A. Hall, *Review nonlinearity in piezoelectric ceramics*, J. Mater. Sci. 36 (2001), pp. 4575–4601.

[11] M. Kamlah and C. Tsakmakis, *Phenomenological modeling of the non-linear electro-mechanical coupling in ferroelectrics*, Int. J. Solids Struct. 36(5) (1999), pp. 669–695.

[12] C.M. Landis, *Non-linear constitutive modeling of ferroelectrics*, Curr. Opin. Solid St. M. 8(1) (2004), pp. 59–69.

[13] D. Zhou and M. Kamlah, *Determination of room-temperature creep of soft lead zirconate titanate piezoceramics under static electric fields*, J. Appl. Phys. 98(10) (2005), pp. 104–107.

[14] D. Zhou and M. Kamlah, Room-temperature creep of soft PZT under static electrical and compressive stress loading, Acta Mater. 54(5) (2006), pp. 1389–1396.

[15] X. Xia, W. Yang, Z. Zheng, and G.J. Weng, *Theory of electric creep and electromechanical coupling with domain evolution for non-poled and fully poled ferroelectric ceramics*, Proc. R. Soc. A 472(2194) (2016), p. 20160468.

[16] M. Kamlah, *Ferroelectric and ferroelastic piezoceramics – Modeling of electromechanical hysteresis phenomena*, Continuum Mech. Therm. 13(4) (2001), pp. 219–268.

[17] S. Stark, P. Neumeister, and H. Balke, *Some aspects of macroscopic phenomenological material models for ferroelectroelastic ceramics*, Int. J. Solids Struct. 80 (2016), pp. 359–367.

[18] S. Lange and A. Ricoeur, *A condensed microelectromechanical approach for modeling tetragonal ferroelectrics*, Int. J. Solids Struct. 54 (2015), pp. 100–110.

[19] B. Kaltenbacher and P. Krejčí, *A thermodynamically consistent phenomenological model for ferroelectric and ferroelastic hysteresis*, ZAMM – J. Appl. Math. Mech./Zeitschrift für Angewandte Mathematik und Mechanik 96(7) (2016), pp. 874–891.

[20] L.T. Wei and D.M. Kochmann, *An effective constitutive model for polycrystalline ferroelectric ceramics: Theoretical framework and numerical examples*, Comp. Mater. Sci. 136 (2017), pp. 223–237.
[21] D. Wang, L.X. Wang, and R. Melnik, *A hysteresis model for ferroelectric ceramics with mechanism for minor loops*, Phys. Lett. A 381(4) (2016), pp. 344–350.
[22] G. Esteves, C.M. Fancher, S. Röhrig, G.A. Maier, J.L. Jones, and M. Deluca, *Electric-field-induced structural changes in multilayer piezoelectric actuators during electrical and mechanical loading*, Acta Mater. 132 (2017), pp. 96–105.
[23] D. Damjanovic, *A morphotropic phase boundary system based on polarization rotation and polarization extension*, Appl. Phys. Lett. 97 (2010), p. 062906.
[24] L.X. Wang and M. Willatzen, Nonlinear dynamical model for hysteresis based on nonconvex potential energy, J. Eng. Mech. 133(5) (2007), pp. 506–513.
[25] M. Iwata and Y. Ishibashi, Phenomenological theory of morphotropic phase boundary with monoclinic phase in solid-solution systems of perovskite-type oxide ferroelectrics, Jpn J. Appl. Phys. 44(5A) (2005), p. 3095.
[26] M. Iwata, Z. Kutnjak, Y. Ishibashi, and R. Blinc, Theoretical analysis of the temperature–field phase diagrams of perovskite-type ferroelectrics, J. Phys. Soc. Jpn 77(3) (2008), p. 034703.
[27] L.X. Wang and M. Willatzen, Extension of the Landau theory for hysteretic electric dynamics in ferroelectric ceramics, J. Electroceram. 24(1) (2010), pp. 51–57.
[28] F. Wolf, A. Sutor, S.J. Rupitsch, and R. Lerch, *Modeling and measurement of creep- and rate-dependent hysteresis in ferroelectric actuators*, Sensor. Actuat. A-Phys 172(1) (2011), pp. 245–252.
[29] M.A. Weber, M. Kamlah, and D. Munz, *Experimentezum Zeitverhalten von Piezokeramiken* [Experiments on the time behavior of piezoceramics]. FZKA, 2000.